Broadband sound generation by confined pulsating jets in a mechanical model of the human larynx

Zhaoyan Zhang[a] and Luc G. Mongeau
Ray W. Herrick Laboratories, Purdue University, 140 South Intramural Drive, West Lafayette, Indiana 47907-2031

(Received 18 July 2005; revised 17 March 2005; accepted 19 March 2006)

Experiments were performed to study the production of broadband sound in confined pulsating jets through orifices with a time-varying area. The goal was to better understand broadband sound generation at the human glottis during voicing. The broadband component was extracted from measured sound signals by the elimination of the periodic component through ensemble averaging. Comparisons were made between the probability density functions of the broadband sound in pulsating jets and of comparable stationary jets. The results indicate that the quasi-steady approximation may be valid for the broadband component when the turbulence is well established and the turbulence kinetic energy is comparatively large. A wavelet analysis of the broadband sound showed that random sound production was modulated at the driving frequency. Two distinct sound production peaks were observed during one cycle, presumably associated firstly with jet formation and secondly with flow deceleration during orifice closing. Most high-frequency sound was produced during the closing phase. Deviations from quasi-steady behavior were observed. As the driving frequency increased, sound production during the opening phase was reduced, possibly due to the shorter time available for turbulence to develop. These results may be useful for better quality voice synthesis. © *2006 Acoustical Society of America.* [DOI: 10.1121/1.2195268]

PACS number(s): 43.70.Bk, 43.28.Ra, 43.70.Aj, 43.28.Py [AL] Pages: 3995–4005

I. INTRODUCTION

Voice production involves sound radiation from pulsating jet flows through the glottis. Air flow from the lung through the subglottal portion of the airway is modulated by quasi-periodic oscillations of the vocal folds. The geometry of the vocal folds varies over one oscillation cycle. The shape of the glottis is in turn divergent, uniform, and convergent. The flow within the glottis during phonation is generally laminar. Turbulence develops immediately downstream the glottis, as a turbulent jet plume develops within the vocal tract. Flow instabilities and large scale vortex shedding may be present, especially when the orifice adopts a divergent shape.

Various sound generating mechanisms contribute to voice production (Zhang *et al.*, 2002b). The three major sound sources are (1) a dipole source consisting of the net unsteady force exerted by the vocal folds walls on the surrounding fluid along the direction of sound propagation in the vocal tract; (2) quadrupole sources due to the components of the fluctuating Reynolds stresses along the direction of sound propagation and associated with flow turbulence within the jet downstream of the glottis in the vocal tract; and (3) a possible monopole source due to flow displaced by the vocal folds walls as they vibrate, characterized by volume changes of the tissue. The dipole source may be further subdivided into two components: (1) a periodic component caused by the flow pulsation through the glottis and (2) a random component caused by turbulent fluctuating pressures acting on the superior vocal folds walls. The periodic component of the dipole sound dominates the radiated sound field and can be accurately modeled using the quasi-steady approximation over most of the duty cycle (Zhang *et al.*, 2002b). The random parts of the dipole sound and the quadrupole sound are random and broadband in nature, and are of smaller amplitude. These components of the radiated sound, however, dominate at high frequencies and contribute to voice quality. In unvoiced sound production, these two components constitute the dominant source of sound (Howe and McGowan, 2005; Krane, 2005). A better understanding of this contribution could help develop better models for speech synthesis and assist in the diagnosis of pathological voice conditions.

The production of broadband sound from air flow through the larynx has been sparsely investigated. In early experiments, Meyer-Eppler (1953) identified a critical Reynolds number below which there was no significant turbulent sound generation, and postulated that the radiated sound pressure increased from that point on with the square of the Reynolds number. Sound production by turbulence in a rigid pipe was investigated by Davies and Ffowcs Williams (1968), who found that the sound power from large-scale turbulence scales with the sixth power of the jet centerline velocity regardless of frequency. Sound power from small-scale turbulence at low frequencies was found to increase with the sixth power of the jet centerline velocity. At high frequency (above the cut-on frequency of the first transverse acoustic mode in the tube), sound power was found to increase with the eighth power of the jet velocity, consistent with the well-known power scaling law of free subsonic jets.

[a]Present address: 31-24 Rehabilitation Center, School of Medicine, UCLA, 1000 Veteran Ave., Los Angeles, CA 90095. Electronic mail: zyzhang@ucla.edu

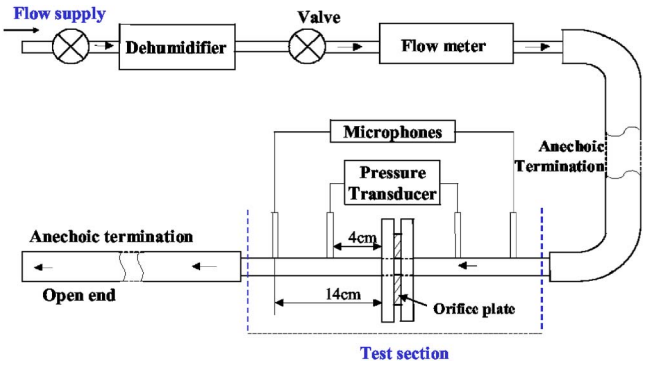

FIG. 1. (Color online) Schematic of the experimental apparatus.

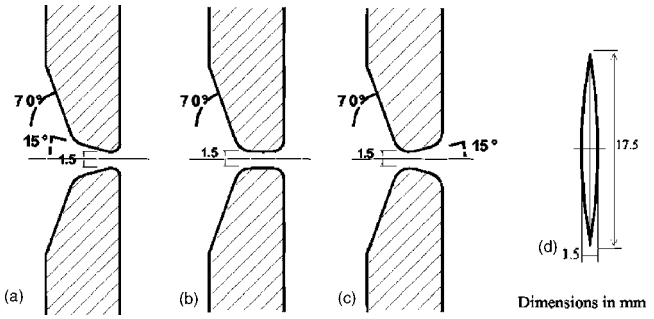

FIG. 2. Coronal cross section of the three orifice passages: (a) convergent, (b) uniform, and (c) divergent. The flow direction is from left (inferior) to right (superior). (d) Geometry of the glottis in the axial plane of minimum constriction.

Recently, sound generation by stationary jet flows through both circular and glottis-shaped fixed orifices in rigid-wall tubes was investigated by Zhang *et al.* (2002a, 2004). Sound power scaling laws that were consistent with those of Davies and Ffowcs Williams were established. The radiated sound power was found to obey a U^6A^2 scaling law at frequencies below the cut-on frequency of higher order acoustic modes in the tubes, where U is the jet centerline velocity and A is the orifice area. Both the quadrupole and dipole sources were found to contribute to sound radiation to varying degrees, depending on the orifice geometry.

Broadband sound radiation in pulsating jet flows has not been studied in detail. The quasi-steady approximation, which has been verified for the periodic component of the voiced sound (Zhang *et al.*, 2000b), may not be valid for the broadband sound component. Production of turbulence was found to be affected by flow acceleration and deceleration (Iguchi *et al.*, 1990). Dabiri and Gharib (2005) studied the transient formation of a vortex ring in a starting flow through nozzles with temporally variable exit diameters. They observed many trends in the flow development for which intrinsically transient mechanisms must be considered. Sound radiation from turbulent pulsating flows is expected to be similarly affected by flow unsteadiness. The combined effects of area modulation and dynamic pressure drops on broadband sound production by pulsating jets have not been investigated before. This question is vital to achieve high-fidelity voice synthesis. In the present study, efforts were made to verify the quasi-steady approximation for the random component of the sound radiated by confined pulsating jets. The probability density function (PDF) of the broadband sound radiated from the pulsating jets was compared to that from comparable stationary jets. Wavelet analysis was used to further investigate the time and frequency characteristics of the broadband sound.

II. EXPERIMENTAL SETUP

A schematic of the experimental facility is shown in Fig. 1. The apparatus was similar to that used in a previous study (Zhang *et al.*, 2002b). A rubber orifice plate was installed between two rectangular tubes. A generic orifice shape was designed with dimensions similar to those of the human glottis. Three orifice profiles (convergent, uniform, and divergent) were used (Fig. 2), each an idealization of the profile of the glottis along a coronal plane mid-way through the vocal folds during phonation. The rubber orifice plate was connected to, and driven by, two electro-dynamic shakers to induce oscillations. The shakers produced displacements sufficiently large to achieve complete closure at frequencies up to 150 Hz. Anechoic terminations were connected to the rectangular test tubes both upstream and downstream to minimize possible sound reflections. The design and performance of the anechoic terminations were described in detail in Zhang *et al.* (2002b). To accurately measure the orifice area, a photoelectric sensor and a light source were installed within the tube walls on opposite sides of the orifice. The photoelectric sensor signal was calibrated by establishing a regression between the output signal of the sensor and the area of the orifice for various shaker plunger positions measured using digital pictures and image processing software (Zhang *et al.*, 2002b). The calibration was repeated before and after the experiments and was verified to be stable during the course of the experiments. The regression between the light sensor output and the orifice area was used for subsequent data processing.

Sound pressures were recorded at two positions located symmetrically upstream and downstream of the orifice, 14 cm away from the orifice discharge plane. The time-averaged volumetric flow rate and the time-averaged pressure gradient across the orifice were measured. A HP356XA data acquisition system was used for the sound pressure measurements. The sampling rate was 32 768 Hz.

III. METHODOLOGY

A. Extraction of the broadband sound component

To decompose the pressure signals into broadband and periodic components, the broadband component was assumed to be random with a zero mean value. The periodic contributions were assumed to be related to the flow pulsation and deterministic. One hundred records of the sound pressure time history at one fixed observation position were recorded. Each record was 1 s long. A trigger signal was used such that each record started at the same time during the orifice oscillation cycle. The periodic component was extracted through synchronous ensemble average. One hundred

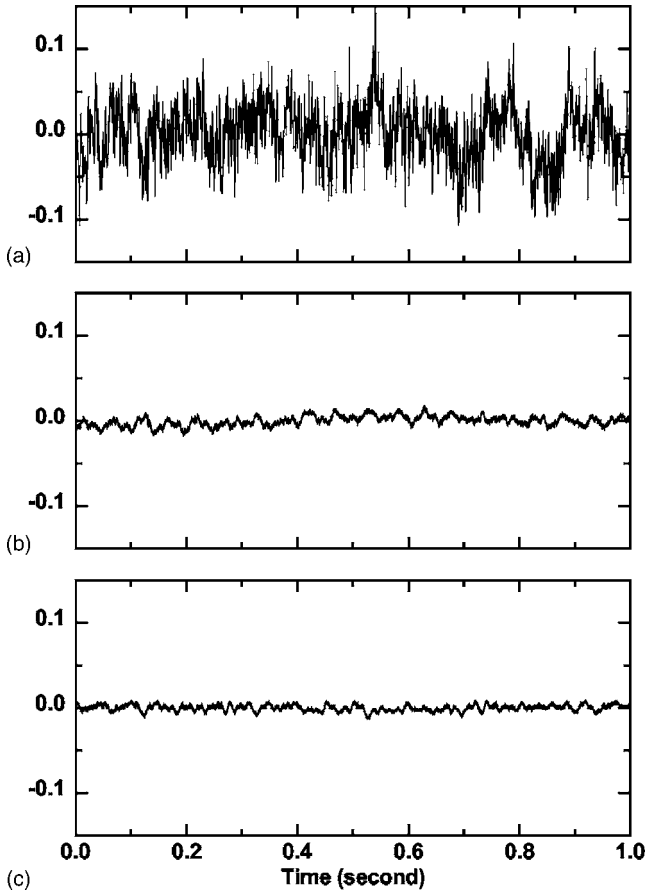

FIG. 3. Sound pressure versus time (a) with flow, periodic component removed; (b) without flow and shaker running and connected to the orifice plate; and (c) measured background noise, without flow, shaker running, but disconnected from the orifice plate. Divergent orifice, $\Delta p_0 = 12$ cm H_2O, $f = 150$ Hz.

samples of the broadband sound component were then obtained by subtracting the periodic component from each original record.

In most of the pulsating flows investigated, the magnitude of the broadband component was much smaller than that of the periodic component. Possible contamination by background mechanical noise due to vibrations of the electro-dynamic shakers was investigated. To evaluate the relative importance of mechanical and aerodynamic noise, the sound pressure associated with the operation of the shakers was measured with the flow supply turned off, and with the orifice either connected or disconnected from the shaker plungers. The results are shown in Fig. 3. Also shown in the figure is the broadband component of the sound obtained using the ensemble-average method for a divergent orifice and a mean pressure of 12 cm H_2O. The broadband sound signal was much greater in magnitude when flow was present than when there was background noise (the signal-to-noise ratio was about 20 for the case shown), which confirmed that the random component of the sound was mostly related to air flow, and not to noise from the operation of the shakers.

B. Probability density function

For a random pressure signal of a finite time interval, T, the probability density function (PDF) was estimated using (Bendat and Piersol, 1986)

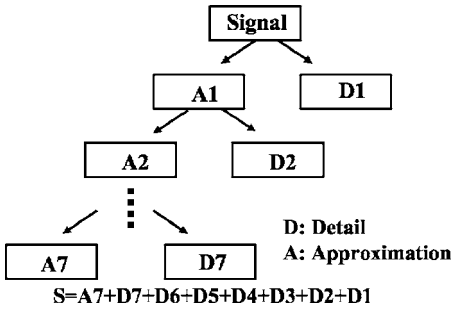

FIG. 4. Illustration of a seven-level discrete wavelet decomposition.

$$f(p) = \frac{T_p(\Delta p)}{T \cdot \Delta p}, \tag{1}$$

where T_p is the total time for which the pressure signal lies within a narrow pressure interval of width Δp centered on p. For comparisons between stationary and pulsating flows, Gaussian distribution regressions of the broadband sound PDFs were performed. The mean value and the standard deviation were estimated. The standard deviation indirectly measures the broadband sound energy. A normalized difference factor was defined to quantify the agreement between PDFs,

$$\varepsilon = \frac{|\sigma_{\text{unsteady}} - \sigma_{\text{steady}}|}{\sigma_{\text{steady}}} \times 100\,\%, \tag{2}$$

where σ_{unsteady} and σ_{steady} are the estimated standard deviations of the broadband sound for pulsating and comparable stationary flows, respectively.

C. Wavelet analysis

The turbulence-generated sound, periodically modulated by the orifice oscillation, is nonstationary in nature and has broad frequency content. Its characteristics in the frequency and time domains were investigated using a wavelet analysis. A wavelet transform produces a time-scale view of a signal, contrasting with the time-frequency view typical of short-time Fourier transforms. This suggests it might be an interesting tool for the analysis of turbulence and turbulence-produced sound, which involve various scales of fluid motions. Wavelets are irregular and transient functions. The mother wavelet is scaled so that it extends over various durations, therefore spanning a flexible window with varying resolution. Higher scales, corresponding to stretched wavelets of longer period and lower frequency, are suitable for the analysis of coarser signal features. Small scales correspond to short durations and they allow the analysis of fine signal features. The wavelet function is shifted over time to analyze local features of signals along the time axis.

The wavelet analysis in this study was performed using the Matlab Wavelet Toolbox. Discrete wavelet decomposition with scales and time positions based on powers of 2 was used. Signals were passed through two complementary filters and decomposed into a detail and an approximation in the time domain, as illustrated in Fig. 4. The two filters are determined by the specified wavelet and act like a low-pass and high-pass filter, respectively. The detail contains the small-

scale high-frequency content of the signal, while the approximation contains larger scale low-frequency information. The detail of level j, D_j, was calculated using (Mallat, 1998; Misiti *et al.*, 2005):

$$D_j(t) = \sum_k C(j,k)\psi_{j,k}(t), \tag{3}$$

where $C(j,k)$ is the discrete wavelet coefficient and $\psi_{j,k}$ is the scaled wavelet. These are defined as

$$C(j,k) = \int_R p(t)\psi_{j,k}(t)dt, \quad \psi_{j,k}(t) = \frac{1}{\sqrt{a}}\psi\left(\frac{t-b}{a}\right), \tag{4}$$

$$a = 2^j,\ b = k2^j,$$

where $p(t)$ is the signal of interest. Scale orders and time steps are denoted by indices j and k, respectively. The approximation of level J, A_J, contains the large-scale component of the original signal:

$$A_J = \sum_{j>J} D_j. \tag{5}$$

The approximation was then passed through the next level wavelet decomposition, using a wavelet of higher scale which is suitable for the analysis of the coarser features left in the approximation, and decomposed into a detail and a higher level approximation. The newly obtained detail and approximation contained again the high- and low-frequency components of the approximation of the previous level, respectively. This process was repeated until the details captured the entire frequency content of the signal under study (Fig. 4).

It should be noted that the two complementary filters were low-pass and high pass filters in terms of scale rather than frequency. Depending on the shape of the wavelet used, various frequency ranges could pass though the low-pass and high-pass filter. The frequency response of these filters can be evaluated by calculating the power spectra of the details and the approximations of white noise passing through the discrete wavelet decomposition. One example is shown in Fig. 5 for the Daubechies 1 (db1) wavelet (Daubechies, 1988). A white noise of normal distribution with a zero mean and unit standard deviation was used. As the scale increased, the frequency of spectral peak values associated with each detail decreased. The peak frequency values for the seven details, in the order of increasing scale, and the seventh approximation were determined from Fig. 5 to be 14 576, 6184, 3072, 1504, 764, 368, 188, and 0 Hz, respectively. For each detail or approximation, several frequency components were included in addition to the main component of energy around the peak frequency.

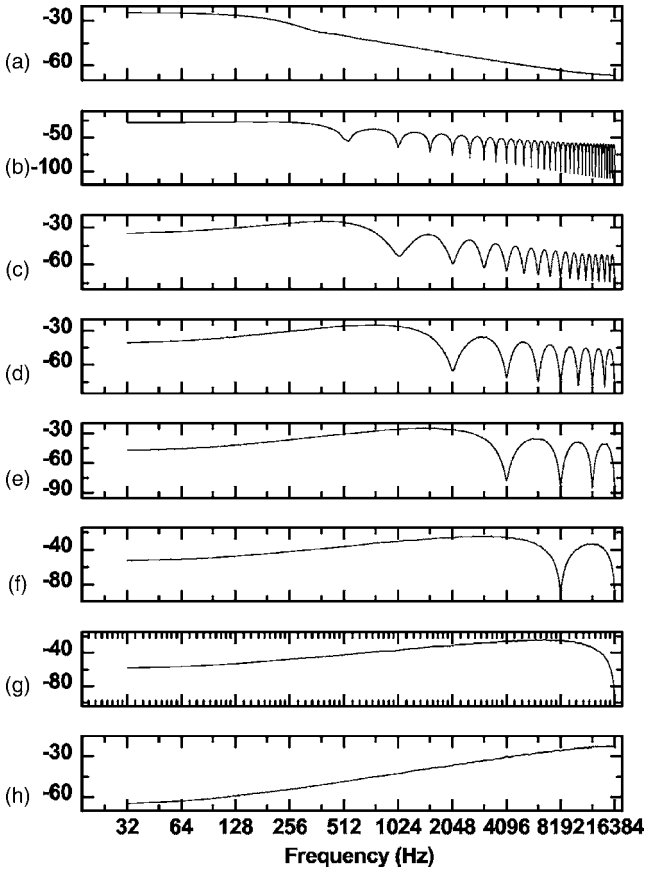

FIG. 5. Power spectra (dB) of the seven-level details and approximations for a white noise input. (a) Seventh approximation; (b) seventh detail; (c) sixth detail; (d) fifth detail; (e) fourth detail; (f) third detail; (g) second detail; and (h) first detail.

IV. RESULTS

A. Probability density functions

The probability density function of the broadband sound was calculated for selected phase values over one cycle in the case of pulsating flows. Additional measurements were then made for stationary flows and fixed orifice, for values of the orifice area and the transglottal pressure matching values recorded in the pulsating flow experiments for the selected phase values over each cycle. Comparisons were made between the sound pressure PDFs of the pulsating flows at specific times over one cycle and comparable stationary flows with the same orifice area and transglottal pressure.

Figure 6 shows the results for the model with a uniform orifice profile driven at 20 Hz. Comparisons were made at six specific instants during one cycle [Figs. 6(a)–6(f)]. These correspond respectively to the beginning of the opening stage (case a), the middle of the opening stage (case b), the end of the opening stage (case c), the beginning of the closing stage (case d), the middle of the closing stage (case e), and the end of the closing stage (case f). These instants are labeled in the corresponding orifice area time history, shown in Fig. 6(g). The normalized difference factors, ε, defined in Eq. (2) are also shown in the figure for each case. Broadband sound production in the pulsating flow case increased as the orifice opened, reached a maximum when the orifice area was nearly maximum, and decreased as the orifice closed. This is qualitatively consistent with the scaling laws for the sound power observed in Zhang *et al.* (2002a), which states that the sound power radiated from stationary jets increases approximately with U^6A^2 at low frequencies, where U is the jet centerline velocity and A is the orifice area.

The agreement between the PDFs in stationary and pulsating flows evolves over one cycle. At the beginning of the

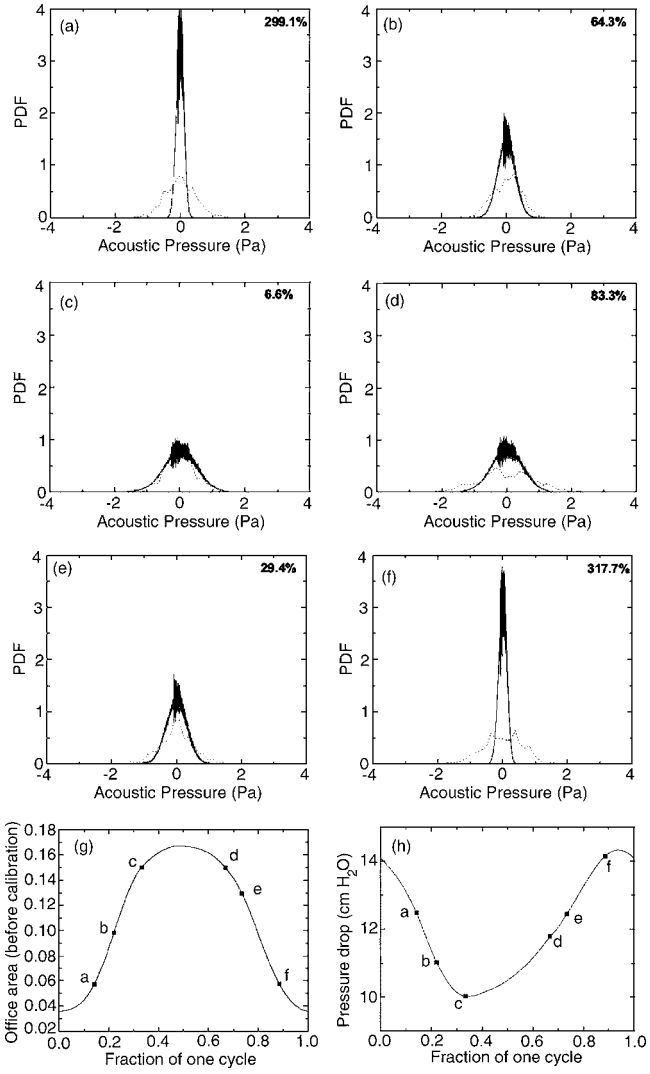

FIG. 6. Probability density function of acoustic pressure for straight orifice driven at 20 Hz. Comparison between the probability density functions of nonstationary and stationary jets was made at six different instants [(a)–(f)] during one orifice oscillation cycle as labeled in panel (g) (orifice area) and panel (h) (transglottal pressure drop).———stationary flow;– –pulsating flow. The number in the upper right corner of panels (a)–(f) quantifies the difference in PDF as defined by Eq. (2).

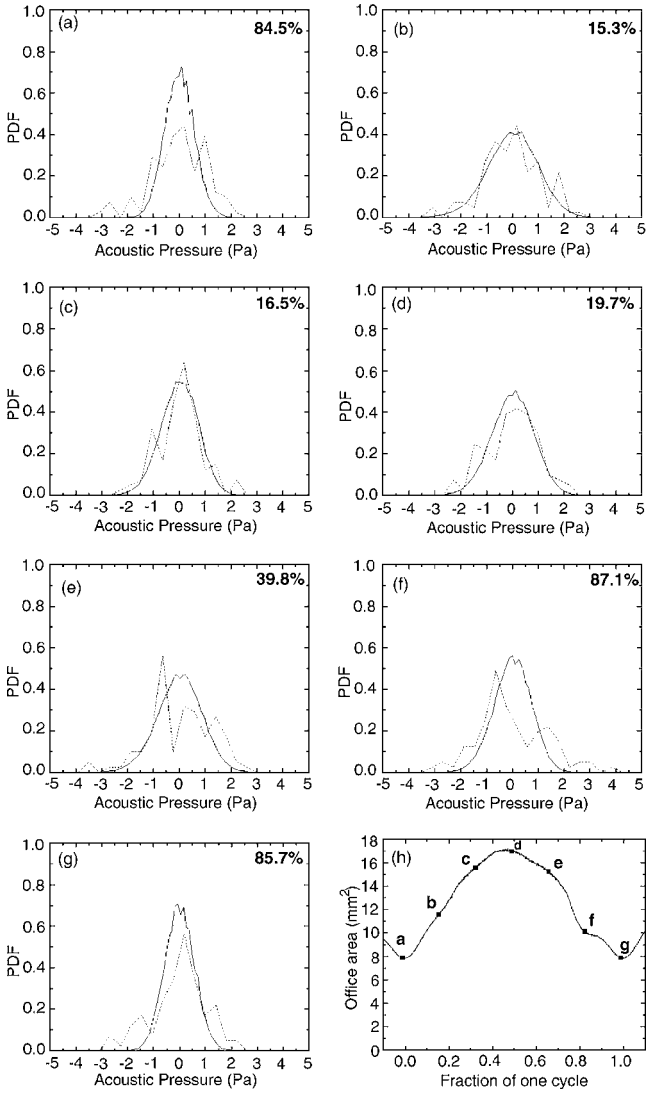

FIG. 7. Probability density function of acoustic pressure for divergent orifice driven at 20 Hz. Comparison between the probability density functions of nonstationary and stationary jets was made at seven different instants [(a)–(g)] during one orifice oscillation cycle as labeled in the orifice area function [panel (h)].———stationary flow;– –pulsating flow. The number in the upper right corner of panels (a)–(g) quantifies the difference in PDF as defined by Eq. (2).

duty cycle (time t_a), the agreement was poor. The PDF in pulsating flows spanned a larger range of acoustic pressure values (or a larger standard deviation) than that in stationary flows, indicating stronger broadband sound production during the opening phase in pulsating flows than in comparable stationary flows. This suggests that the unsteady effects played an important role in the broadband sound production at that time. The unsteadiness of flow was generally greater during the acceleration and deceleration stages than over the middle of the cycle when the flow was apparently into a quasi-stationary state. It is also possible that the effects of persisting vortical structures from the previous cycle may not have been completely dissipated before the beginning of a new cycle, resulting in more broadband sound production than that for a comparable stationary flow. The agreement between the PDFs for stationary and pulsating flows improved as the orifice area increased (at time t_b), after the flow was better established. The best agreement was obtained at time t_c, at which the orifice opening was nearly maximum and the turbulence energy was most probably nearly maximum. During the closing stage of the duty cycle, the agreement was less good (at times t_d and t_e). For time t_f, near the end of the cycle, the flow rate was small and the PDFs were in poor agreement. Note that the broadband sound amplitudes were almost always larger in pulsating flows than that in comparable stationary flows.

Figures 7–9 show similar results for a divergent orifice driven at 20, 100, and 200 Hz, respectively. Figure 10 shows the results for a convergent orifice driven at 100 Hz. Similar observations can be made for all these cases. The quasi-steady approximation was only valid during part of the oscillation cycle. The agreement between the PDF for pulsating and stationary flows was generally poor when the orifice area was nil or small. The agreement improved as the orifice area increased, and the best agreement was generally obtained

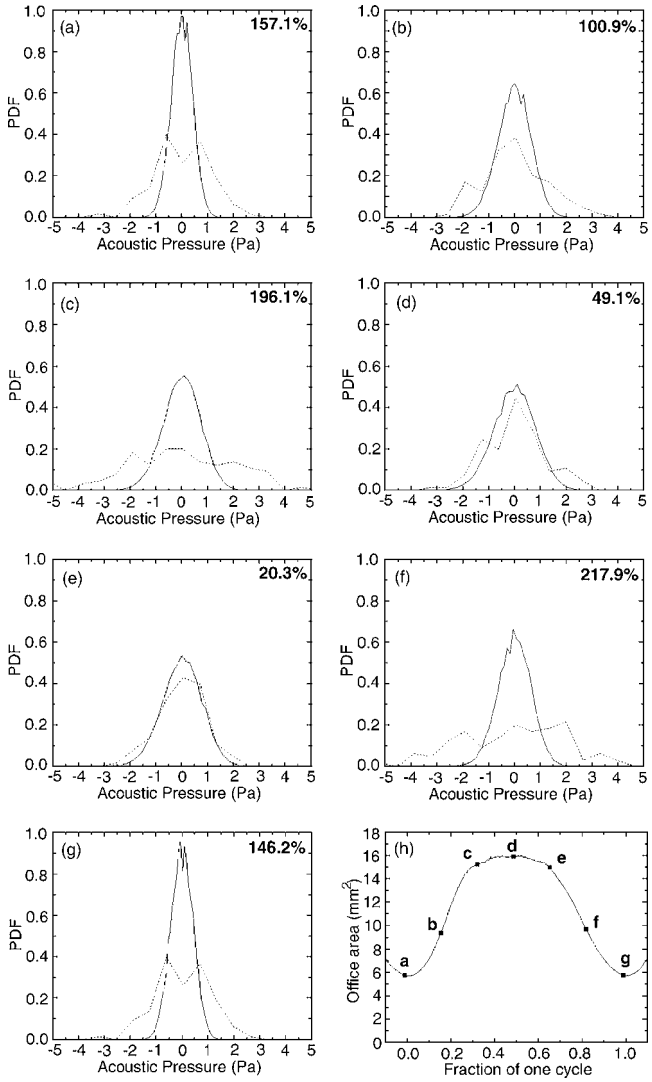

FIG. 8. Probability density function of acoustic pressure for divergent orifice driven at 100 Hz. Comparison between the probability density functions of nonstationary and stationary jets was made at seven different instants [(a)–(g)] during one orifice oscillation cycle as labeled in the orifice area function [panel (h)].———stationary flow;– –pulsating flow. The number in the upper right corner of panels (a)–(g) quantifies the difference in PDF as defined by Eq. (2).

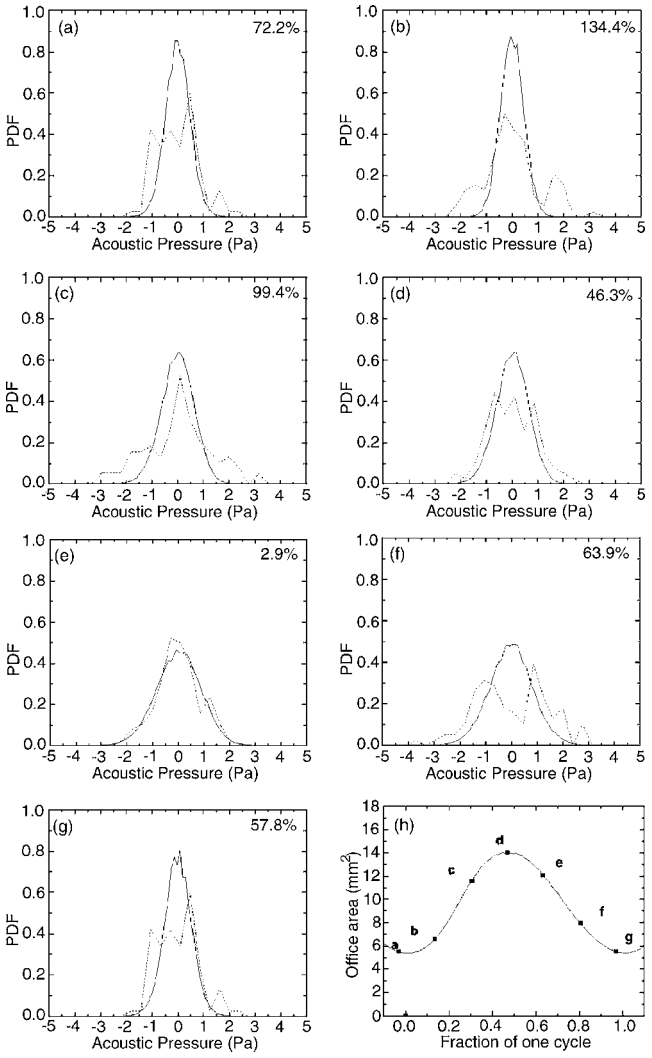

FIG. 9. Probability density function of acoustic pressure for divergent orifice driven at 200 Hz. Comparison between the probability density functions of nonstationary and stationary jets was made at seven different instants [(a)–(g)] during one orifice oscillation cycle as labeled in the orifice area function [panel (h)].———stationary flow;– –pulsating flow. The number in the upper right corner of panels (a)–(g) quantifies the difference in PDF as defined by Eq. (2).

when the orifice opening was nearly maximum. Although not as apparent as in Fig. 6, there was generally more broadband sound production in pulsating flows than that in comparable stationary flows during acceleration and deceleration, indicating the important role played by the flow unsteadiness.

The centerline jet velocity was almost constant over the duty cycle, except in the early phases of jet development and quenching (Mongeau *et al.*, 1997; Zhang, 2002). An increase in frequency increases the excitation Strouhal number and, therefore, in theory, the possible influence of unsteady effects. However, no significant and consistent influence of the driving frequency on the agreement between the PDFs of pulsating and comparable stationary flows (Figs. 7–9) was observed in the experiments. This may be because the driving frequency was not high enough to have a significant effect on the development of large-scale turbulence, which contributes the most to the total broadband sound. The driving frequency is also expected to have an impact on small-scale turbulent structures and their contribution to the broadband sound production, as discussed further in the next section.

The large fluctuations in the PDF for the pulsating jets were partially due to the limited number of averages. Another potential source of errors was a small drift in the orifice area history over time due to slight relaxation of the rubber orifice plates, which may have caused variability during the experiments. In particular, slight changes in duty cycle and collision times between the two vocal folds could have made the flow and the sound radiation vary slightly from cycle to cycle. This would lead to errors in the ensemble-averaging process. Evidence of this type of error is apparent in Fig. 8(f), in which a periodic component was present in the sound signals. This points out at the possibility that the periodic component may not have been completely removed in that particular case.

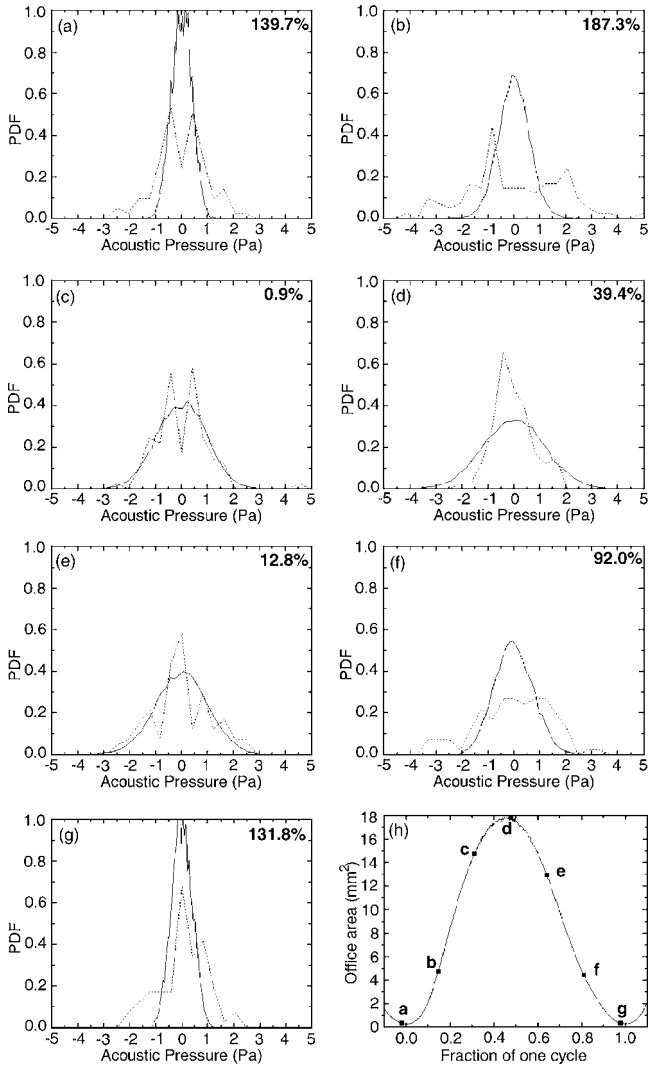

FIG. 10. Probability density function of acoustic pressure for convergent orifice driven at 100 Hz. Comparison between the probability density functions of nonstationary and stationary jets was made at seven different instants [(a)–(g)] during one orifice oscillation cycle as labeled in the orifice area function [panel (h)].———stationary flow;– –pulsating flow. The number in the upper right corner of panels (a)–(g) quantifies the difference in PDF as defined by Eq. (2).

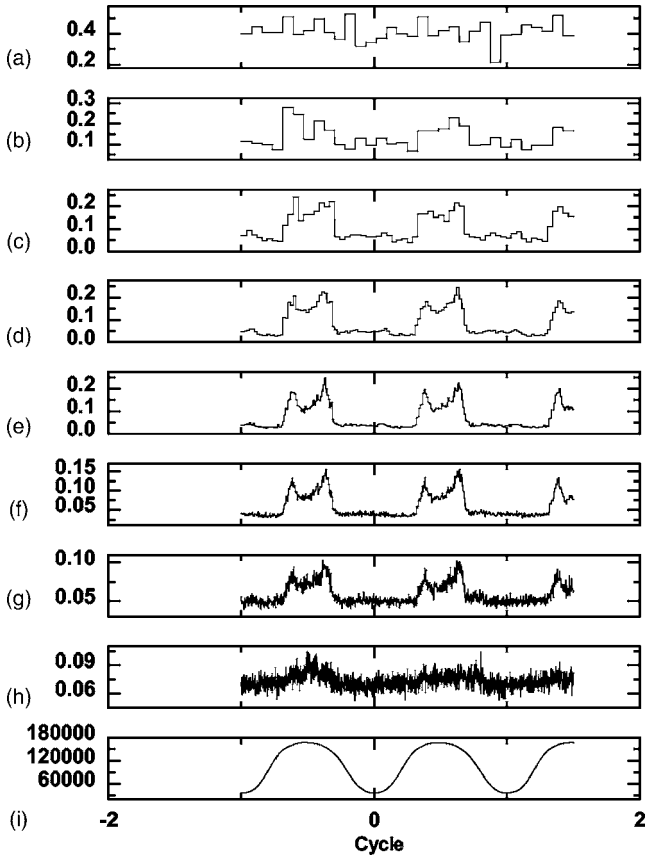

FIG. 11. Wavelet decomposition of the broadband sound generated by pulsating confined jets through straight orifice driven at 20 Hz. (a) Seventh approximation; (b) seventh detail; (c) sixth detail; (d) fifth detail; (e) fourth detail; (f) third detail; (g) second detail; (h) first detail, and (i) orifice area function in arbitrary unit.

B. Wavelet analysis

Broadband sound produced by turbulence includes contributions from turbulent structures of varying length and time scales, each corresponding to a characteristic frequency distinct from that of the periodic component. Sound production by turbulent structures of different scales during one oscillation cycle was investigated using wavelet analysis. The Daubechies 1 wavelet, which resembles a step function, was used in this study. A seven-level discrete wavelet transform was applied to each broadband sound record. The resulting details and approximations were then ensemble averaged on an energy basis to obtain mean values.

Figure 11 shows the wavelet coefficients for the broadband component of the sound obtained for a uniform orifice driven at 20 Hz, with $\Delta p = 12$ cm H_2O. The details of each level and the approximation at the seventh level are shown. Also shown is the orifice area [Fig. 11(i)]. No corrections were made to account for time delays due to either flow convection or sound propagation and reflection. The amplitude of each detail and approximation measured the sound energy at each scale and time value. Significant sound energy was present at very large scales or low frequencies (the seventh approximation). This is consistent with the high sound level at low frequencies in the stationary jets sound spectra and was attributed to local turbulent pressure fluctuations over the microphones (Zhang *et al.*, 2002a). The turbulent sound energy decreased monotonically with the nominal frequency. The wavelet coefficients at all levels featured a modulating envelope which had the same frequency as the orifice oscillation. During one cycle, sound energy was significant only over the part of the cycle at which the orifice area was nearly maximum. A threshold value existed in the orifice area below which sound radiation was negligible. In pulsating jet flows, the turbulence-generated sound is equal to the rate of change in the axial kinetic energy in the source region (Zhao *et al.*, 2001). Thus, the total axial kinetic energy change in the source region due to the flow pulsation acts as a low-frequency quadrupole source, which may give rise to the modulation at the driving frequency shown in Fig. 11.

For intermediate scales, the wavelet coefficients culminated twice over each cycle, shortly before and after the instant of maximum orifice area. The first peak appeared to be associated with the developing part of the jet. The second

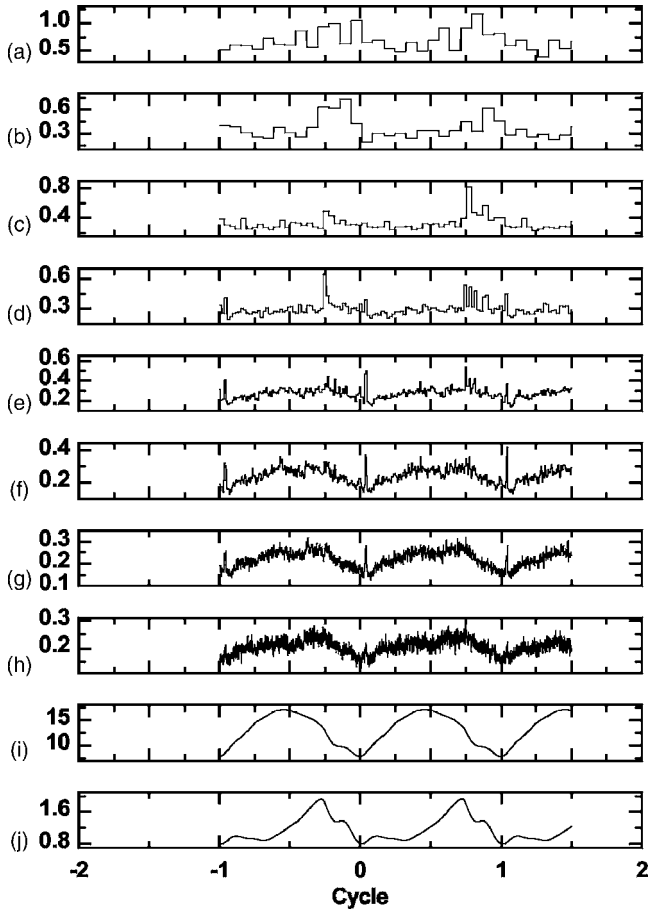

FIG. 12. Wavelet decomposition of the broadband sound generated by pulsating confined jets through divergent orifice driven at 20 Hz. (a) Seventh approximation; (b) seventh detail; (c) sixth detail; (d) fifth detail; (e) fourth detail; (f) third detail; (g) second detail; (h) first detail; (i) orifice area function in mm^2; and (j) U^6A^2.

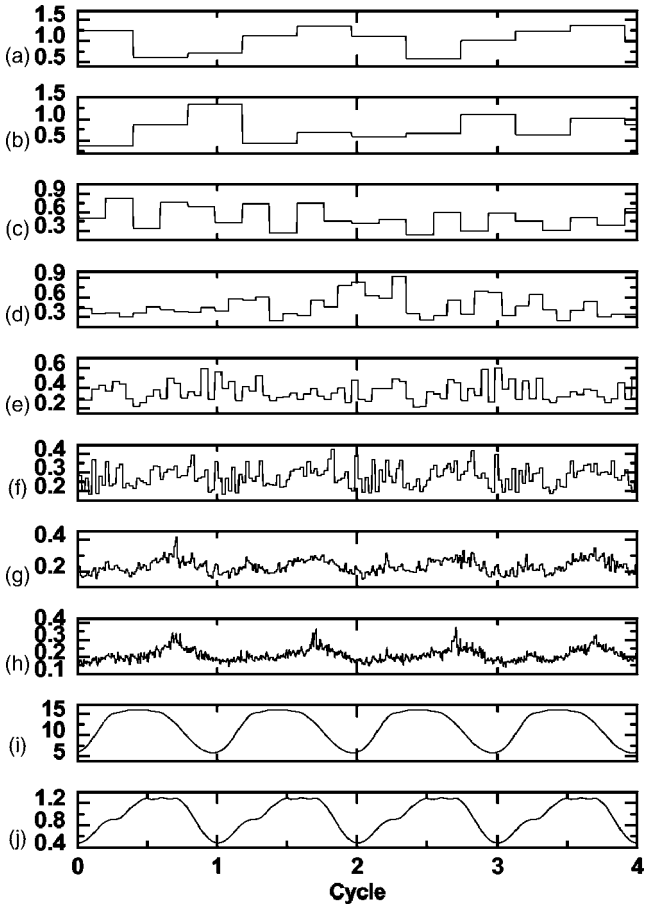

FIG. 13. Wavelet decomposition of the broadband sound generated by pulsating confined jets through divergent orifice driven at 100 Hz. (a) seventh approximation; (b) seventh detail; (c) sixth detail; (d) fifth detail; (e) fourth detail; (f) third detail; (g) second detail; (h) first detail; (i) orifice area function in mm^2; and (j) U^6A^2.

peak was associated with the quenching of the flow during orifice closing. Asymmetric behavior about the instant of the maximum orifice opening was observed, especially at small scales or high frequencies. The second peak was slightly delayed in time, and its amplitude was slightly larger than that of the first peak. For small-scale (high-frequency) components [e.g., the first detail in this case, Fig. 11(h)], the first peak was smaller in amplitude than that for the larger scales, indicating lower high-frequency sound production compared with the mid-frequency components during the opening stage (or the jet formation stage). This may indicate that the small-scale flow structures need more time to develop than the underlying large scale flow.

Figure 12 shows the wavelet decomposition for the case of a divergent orifice driven at 20 Hz. The orifice displacement was very small, and thus the orifice was open during the entire cycle. The details again show a modulation at the driving frequency. The two peaks are still discernable, although not so clearly. Also shown in the figure [Fig. 12(j)] is the sound power scaling law U^6A^2 developed in Zhang *et al.* (2002a) for low frequencies. This scaling law, describing the sound power produced in stationary flow, would yield a first approximation of the sound power produced over one cycle in pulsating flows. Neither the scaling law nor the orifice area history was in good agreement with the wavelet details, indicating again that the broadband sound generation process may not be perfectly quasi-steady. However, the U^6A^2 scaling law was generally in better agreement with the wavelet details than with the orifice area. Considering the non-quasi-steady behavior discussed in the previous section, the peaks in the U^6A^2 scaling law coincided approximately with the peaks in the details of the wavelet decomposition. This is particularly true for the high level of details [compare Fig. 12(b) with 12(j)]. The high level of detail corresponds to the dominant contributions from large-scale turbulence and appears to be a good indicator of sound power.

The experiments were repeated at higher frequencies, more typical of voice production. Figures 13 and 14 show the wavelet decomposition for a divergent orifice driven at 100 and 200 Hz, respectively. Figure 15 shows the wavelet decomposition for a convergent orifice driven at 100 Hz. The low-frequency modulation was present for all cases, except in the high level of detail for the case of the divergent orifice driven at 100 Hz. As discussed earlier, the periodic component may not be completely removed by the ensemble-averaging process for this case. The wavelet details showed two peaks over one cycle for intermediate scales. The first peak, within the opening stage, gradually disappeared as the

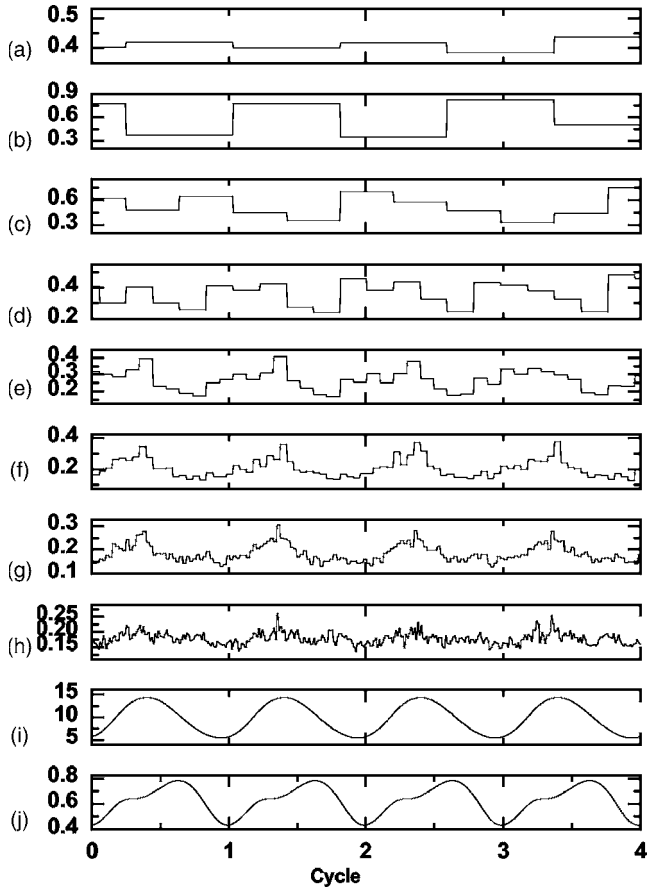

FIG. 14. Wavelet decomposition of the broadband sound generated by pulsating confined jets through divergent orifice driven at 200 Hz. (a) seventh approximation; (b) seventh detail; (c) sixth detail; (d) fifth detail; (e) fourth detail; (f) third detail; (g) second detail; (h) first detail; (i) orifice area function in mm^2; and (j) U^6A^2.

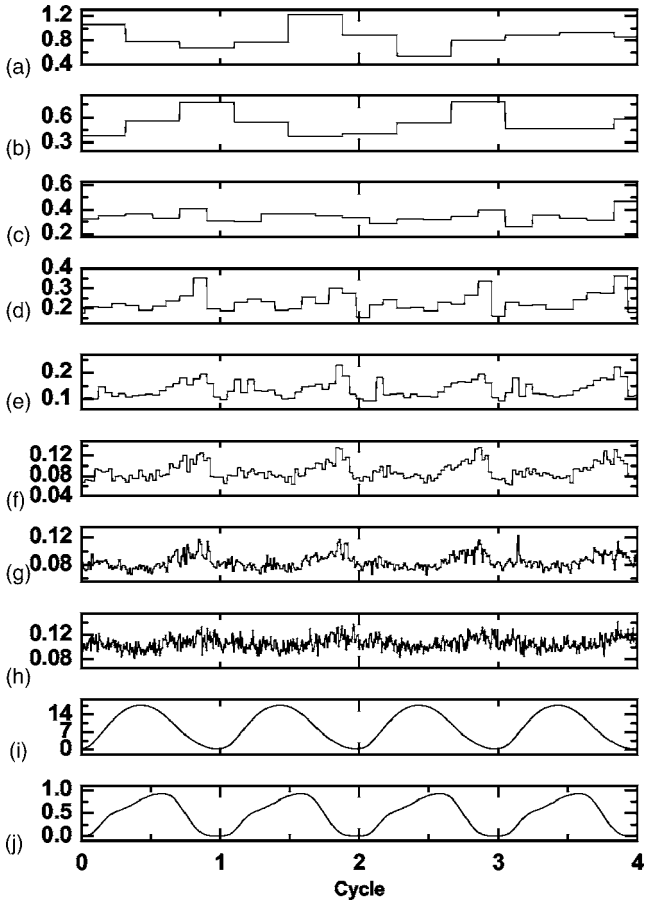

FIG. 15. Wavelet decomposition of the broadband sound generated by pulsating confined jets through convergent orifice driven at 100 Hz. (a) seventh approximation; (b) seventh detail; (c) sixth detail; (d) fifth detail; (e) fourth detail; (f) third detail; (g) second detail; (h) first detail; (i) orifice area function in mm^2; and (j) U^6A^2.

frequency increased. The general shape of the wavelet details matched the scaling law U^6A^2 better than the orifice area function.

For the same level of details, the first peak was less apparent as the driving frequency was increased. This indicates that at frequencies typical of voice production, the turbulent field, especially the fine-scale structures, may not have enough time to fully establish itself. Most of the turbulence sound at high frequencies was produced during the orifice closing stage. No jet tones were observed for jet flows through a divergent orifice, in contrast to that observed in the case of stationary jets (Zhang *et al.*, 2004). Those feedback mechanisms responsible for the jet tones may not have enough time to lock in for pulsating flows (Pelorson *et al.*, 1994).

Note that for the case of the divergent orifice and 200 Hz, the details were slightly ahead of the orifice area function in shape. This misalignment was probably due to delays associated with acoustic propagation and flow convection, which were not accounted for and may be important at high driving frequencies.

The analysis above has been repeated using other wavelet functions. Although details differ, qualitatively similar results were obtained. It is possible that some wavelets are more appropriate than others in this particular application. However, this is beyond the scope of this study and was not investigated further.

V. DISCUSSION

A major difference between the mechanical model and human phonation is that the motion of the vocal fold model in this study was imposed independently of the flow field and the acoustical environment, rather than induced by the glottal flow as in the case of human phonation. The deformation amplitude of the rubber vocal fold model was limited. The fluid-structure interactions within the human glottis were therefore not reproduced in the driven physical model. Such interaction may help to smooth the glottis motion, especially during orifice opening and closing, therefore reducing flow unsteadiness. The flow in real speech may not be as unsteady as it is in the mechanical model. This issue will be further investigated using more realistic vocal fold models.

Complete orifice closure was not always achieved in the experiments. Incomplete closure of the orifice implies that there is always a mean flow through the orifice. The possible effects of a nonzero mean flow on the broadband sound production and the validity of the quasi-steady approximation were not investigated in this study. The presence of a mean

flow might increase the radiated broadband sound energy during the initial opening and final closing stages, due to the persisting turbulent structures downstream in the vocal tract through the entire oscillating cycle, as compared to the case of total orifice closure. Small-scale turbulence would likely have more time to develop when a mean flow is present, leading to more sound production at high frequencies. However, this effect may be counteracted by the reduced flow unsteadiness due to the reduced orifice vibration amplitude, other experimental parameters remaining unchanged. This is particularly true in the initial opening and final closing stages, during which the flow unsteadiness boosts the broadband sound production as shown in this study. On the other hand, reduced flow unsteadiness implies that the quasi-steady models should better predict the broadband sound production than in the case of complete orifice closure. In the extreme case, when the oscillation amplitude is very small (e.g., in a falsettolike vibration), the flow is expected to be predicted well by using the quasi-steady approximation.

Although deviations from the quasi-steady approximation were observed in the broadband sound production, the scaling law for sound power (U^6A^2) developed in previous stationary flow studies qualitatively predicted the unsteady broadband sound production during one oscillation cycle. This scaling law for the sound power and the scaling law for the source spectral function (Zhang *et al.*, 2002a) may be used for noise modeling in high-quality synthesis of normal and pathological voices. To implement the broadband sound component, each glottal oscillation cycle may be subdivided into short-duration time segments. A typical velocity and diameter may then be assigned to each time segment, with their values determined from the harmonic source (either a prescribed pulse train or derived from speech signals using inverse filtering) during the corresponding time segment. Spectral filters can then be designed from the typical velocity, diameter, and the appropriate spectral similarity law developed in Zhang *et al.* (2002a). For each time segment, a random white noise of longer duration is passed through the corresponding spectral filter and a constituent broadband sound is generated. The final broadband sound is obtained by assembling these short segments of the constituent broadband sounds, properly scaled, in sequence. The unsteady effects (deviations from the quasi-steady approximation) can be accounted for by introducing a scaling factor for each time segment. The resulting broadband sound could then be superimposed onto the periodic sound component. Others models such as the Meyer-Eppler model could be also implemented. Comparisons between the qualities of the resulting voice output from these two models as well as original speech signals may be used to evaluate the effectiveness of the developed sound power and spectral similarity laws.

VI. CONCLUSIONS

Experiments were performed to study the characteristics of broadband sound generation by confined pulsating jets. The broadband sound component was isolated from measured sound signals by the method of ensemble averaging. The probability density function (PDF) of the broadband sound was calculated and compared to that of the sound radiated from a stationary jet flow with the same orifice area for the same flow boundary conditions. A good agreement was obtained between the PDF of the pulsating jets and the stationary jets at instants during one cycle when the orifice area was close to its maximum value. Discrepancies between the PDFs at the initial and ending stages of the orifice oscillating cycle were observed due to flow acceleration and deceleration. This indicates that the quasi-steady approximation may be valid for the broadband component when the turbulence is well established and the turbulence energy is comparatively large.

A wavelet analysis (seven-level discrete wavelet transform using the Daubechies 1 wavelet) of the broadband sound showed that random sound production was modulated at the driving frequency. Although deviations from quasi-steady approximation were observed, the scaling law for sound power developed in previous studies matched qualitatively the general shape of the sound production by the large-scale turbulence during one orifice cycle. Dual peaks in the wavelet coefficients were observed during one cycle for the orifice area near its maximum value. The first peak was most likely associated with jet formation, while the second was associated with flow deceleration during orifice closing. The first peak became less apparent at high frequency, suggesting that there was very little small-scale or high-frequency sound production during the opening phase. Increased driving frequency was found to have more impact on sound from small-scale turbulence than that from large-scale components. As the driving frequency increased, sound production during the opening stage was also reduced due to the shorter time available for turbulence to develop.

ACKNOWLEDGMENT

This study was supported by Research Grant No. RO1 DC03577 from the National Institute of Deafness and Other Communication Disorders, National Institutes of Health.

Bendat, J. S., and Piersol, A. G. (**1986**). *Random Data: Analysis and Measurement Procedures* (Wiley, New York).

Dabiri, J. O., and Gharib, M. (**2005**). "Starting flow through nozzles with temporally variable exit diameter," J. Fluid Mech. **538**, 111–136.

Daubechies, I. (**1988**). "Orthonormal bases of compactly supported wavelets," Commun. Pure Appl. Math. **41**, 909–996.

Davies, H. G., and Ffowcs Williams, J. E. (**1968**). "Aerodynamic sound generation in pipe," J. Fluid Mech. **32**(4), 765–778.

Howe, M. S., and McGowan, R. S. (**2005**). "Aeroacoustics of [s]," Proc. R. Soc. London, Ser. A **461**, 1005–1028.

Iguchi, M., Yamazaki, H., Yamada, E., and Morita, Z. (**1990**). "Velocity and turbulence intensity in a pulsating jet through a sudden expansion," Trans. Jpn. Soc. Mech. Eng., Sec. B **56**, 1659–1664.

Krane, M. H. (**2005**). "Aeroacoustic production of low-frequency unvoiced speech sounds," J. Acoust. Soc. Am. **118**, 410–427.

Mallat, S. G. (**1998**). *A Wavelet Tour of Signal Processing* (Academic, San Diego).

Meyer-Eppler, W. (1953). "Zum Erzeugungsmechanismus der Geräuschlaute (On the production mechanism of the obstruent sounds)," Z. Phonetik und allgemeine Sprachwissenschaft (Journal of Phonetics and Linguistics) **7**, 196–212.

Misiti, M., Misiti, Y., Oppenheim, G., and Poggi, J. M. (**2005**). *Wavelet Toolbox User's Guide* (The MathWorks, Inc., Natick, MA).

Mongeau, L., Franchek, N., Coker, C. H., and Kubli, R. A. (**1997**). "Characteristics of a pulsating jet through a small modulated orifice, with application to voice production," J. Acoust. Soc. Am. **102**, 1121–1133.

Pelorson, X., Hirschberg, A., van Hassel, R. R., Wijnands, A. P. J., and Auregan, Y. (**1994**). "Theoretical and experimental study of quasisteady-flow separation within the glottis during phonation. Application to a modified two-mass model," J. Acoust. Soc. Am. **96**, 3416–3431.

Zhang, Z. (2002). "Experimental study of sound generation by confined jets with application to human phonation," Ph.D. thesis, Purdue University, West Lafayette, IN.

Zhang, Z., Mongeau, L., and Frankel, S. H. (**2002a**). "Broadband sound generation by confined turbulent jets," J. Acoust. Soc. Am. **112**(2), 677–689.

Zhang, Z., Mongeau, L., and Frankel, S. H. (**2002b**). "Experimental verification of the quasi-steady approximation for aerodynamic sound generation by pulsating jets in tubes," J. Acoust. Soc. Am. **112**(4), 1652–1663.

Zhang, Z., Mongeau, L., Frankel, S. H., Thomson, S., and Park, J. (**2004**). "Sound generation by steady flow through glottis-shaped orifices," J. Acoust. Soc. Am. **116**(3), 1720–1728.

Zhao, W., Frankel, S. H., and Mongeau, L. (**2001**). "Numerical simulations of sound from confined pulsating axisymmetric jets," AIAA J. **39**(10), 1868–1874.